metals

MDPI

Article

Influence of Rare Earth Oxide Concentration on Electrochemical Co-Deposition of Nd and Pr from NdF_3-PrF_3-LiF Based Melts

Vesna S. Cvetković [1,*], Dominic Feldhaus [2], Nataša M. Vukićević [1], Ksenija Milicevic-Neumann [2], Tanja S. Barudžija [3], Bernd Friedrich [2] and Jovan N. Jovićević [1]

[1] Department of Electrochemistry, Institute of Chemistry, Technology and Metallurgy, National Institute of the Republic of Serbia, University of Belgrade, 110000 Belgrade, Serbia; vukicevic@ihtm.bg.ac.rs (N.M.V.); jovicevic@ihtm.bg.ac.rs (J.N.J.)

[2] IME Process Metallurgy and Metal Recycling, Institute of RWTH Aachen University, 52056 Aachen, Germany; dfeldhaus@metallurgie.rwth-aachen.de (D.F.); kmneumann@metallurgie.rwth-aachen.de (K.M.-N.); bfriedrich@metallurgie.rwth-aachen.de (B.F.)

[3] Institute for Nuclear Sciences Vinča, University of Belgrade, 11001 Belgrade, Serbia; tbarudzija@vin.bg.ac.rs

* Correspondence: v.cvetkovic@ihtm.bg.ac.rs

Abstract: The impact of rare earth oxide (REO) concentration on the deposition process and selective recovery of the metal being deposited from a molten fluoride salt system was investigated by applying deposition of Nd and Pr and varying the concentration of REO added to the electrolyte. A ternary phase diagram for the liquidus temperature of the NdF_3-PrF_3-LiF system was constructed to better predict the optimal electrolyte constitution. Cyclic voltammetry was used to record three redox signals, reflecting the processes involving Nd(III)/Nd and Pr(III)/Pr transformations. A two-step red/ox process for Nd(III) ions and a single-step red/ox process for Pr(III) ions were confirmed by square-wave voltammetry. The cyclic voltammetry results indicated the possibility of neodymium and praseodymium co-deposition. In order to sustain higher co-deposition rates on the cathode and to avoid increased production of PFC greenhouse gases on the anode, a low-overpotential deposition technique was used for Nd and Pr electrodeposition from the electrolyte with varying Nd_2O_3 and Pr_6O_{11} concentrations. Co-deposited neodymium and praseodymium metals were characterized by electron probe microanalysis (EPMA) and X-ray diffraction (XRD) analysis. After electrodeposition, concentration profiles of neodymium and praseodymium were recorded, starting from the cathode surface towards the electrolyte bulk. The working temperature of 1050 °C of the molten fluoride salt basic electrolyte, in line with the constructed phase diagram, was validated by improved co-deposition and led to a more effective deposition process.

Keywords: Nd; Pr; co-deposition; fluoride melts; ternary phase diagram; EPMA; XRD

check for updates

Citation: Cvetković, V.S.; Feldhaus, D.; Vukićević, N.M.; Milicevic-Neumann, K.; Barudžija, T.S.; Friedrich, B.; Jovićević, J.N. Influence of Rare Earth Oxide Concentration on Electrochemical Co-Deposition of Nd and Pr from NdF_3-PrF_3-LiF Based Melts. *Metals* **2022**, *12*, 1204. https://doi.org/10.3390/met12071204

Academic Editors: Chang Woo Lee and Felix A. Lopez

Received: 27 May 2022
Accepted: 13 July 2022
Published: 15 July 2022

Publisher's Note: MDPI stays neutral with regard to jurisdictional claims in published maps and institutional affiliations.

Copyright: © 2022 by the authors. Licensee MDPI, Basel, Switzerland. This article is an open access article distributed under the terms and conditions of the Creative Commons Attribution (CC BY) license (https://creativecommons.org/licenses/by/4.0/).

1. Introduction

Rare earth elements (REEs) have been widely employed in diverse industrial materials, owing to their unique magnetic, phosphorescent, physical and catalytic properties [1]. They became important ingredients in various compounds, and consequently, global demand for rare earth products increased exponentially, particularly in energy-efficient functional materials, such as neodymium–iron–boron (NdFeB) magnets [2,3]. From the viewpoint of sustainability, in the coming decades, with the push towards cleaner and greener future, supply channels will evidently face difficulties in meeting the growing demand for REEs [4,5].

Continuous growth of solid waste containing rare earth elements is generating a lot of interest in recycling and recovery technologies for these elements from used industrial materials. Development and implementation of such technologies are expected to assume a very important role in supplementing virgin REE production in supply chains. Electrochemical deposition has proven to be a capable alternative in selective recovery of a

desired element from an electrolyte containing mixed rare earth ions [3,6–9]. The ability to monitor and control the deposition process, composition, morphology and especially the purity of the final products are some of the advantages attributed to the electrolytic production method.

The electrochemical behaviour of selected metal ions in an electrolyte system were studied to achieve energy-efficient recovery of rare earth metals [10]. These fundamental studies were aimed at providing a basis for REE electrolytic production and refining from relevant secondary resources. Selective electrolytic production of RE elements (RE = Nd, Pr or Dy) alone or RE alloys using an appropriate working substrate by electrolysis from fluoride or chloride molten salts system have been studied to some extent [2,5,11–16]. Significant work has been done concerning the electrochemistry of each element separately or as part of a group in the corresponding molten salt mixture using molten salt electrochemistry [6,7,11,17–20]. However, there has been little related research conducted on selective neodymium/praseodymium electrochemical deposition from oxide-fluoride electrolytes [6–8,21–23]. Currently, industrial production of Nd-Pr alloys is mostly based on the electrochemical processes of oxide-fluoride electrolytes, using PrF_3-NdF_3-LiF as the base electrolyte and Nd and Pr oxides as a feedstock. Therefore, experiments have been continuously conducted to improve knowledge of these processes. For example, a study on the solubility of Pr and Nd oxides in their corresponding LiF–REF electrolytes was conducted by online monitoring of the oxide concentration during rare earth metal electrowinning [8]. Recently, relationships between conductivity of molten PrF_3-NdF_3-LiF-Pr_6O_{11}-Nd_2O_3 salt and varied temperature, LiF content or REO concentration were identified in the system [22].

Data concerning the potential environmental risk associated with the RE production via electrodeposition from molten salts are rather scarce. A study was conducted on the electrode reactions on the carbon anode in fluoride based molten salts containing RE oxides. The authors reported that during the electrolysis of didymium from oxide-fluoride molten salts, emission of carbon oxides and perfluorocarbon gasses depended on oxide concentration and deposition current density [24].

Despite the efforts made to date, there are still a number of remaining challenges, such as the melting temperature of the electrolyte, the effect of LiF and/or REO addition to the electrolyte composition, parameters that play an important role in controlling the entire rare earth element electrolysis process. Phase diagrams are a useful tool for understanding the investigated system and the present phases, as well as their states and melting temperatures. Studies addressing the phase diagrams of neodymium and praseodymium fluoride salts as base electrolytes in the molten salt electrolysis process for REE production are scarce. The binary phase diagrams of NdF_3-LiF and PrF_3-LiF were reported by Thoma [25], as well as Berkani and Gaune-Escard [26], whereas the ternary phase diagram was reported by Liu [27]. Liu used previously available binary system data, and combined it with limited experimental results for liquidus temperature measured by differential scanning calorimetry (DSC).

Recently, we successfully employed a fluoride based molten PrF_3-NdF_3-LiF bath as a solvent for neodymium and praseodymium oxides and as an electrolyte for the electrodeposition of Nd and Pr metals on an inert working substrate [6,7,17]. Our study was focused on the fundamentals underlying the electrochemical reduction of both Nd(III)/Nd(0) and Pr(III)/Pr(0) cations that occurs in the oxide-fluoride melt using a glassy carbon counter electrode (anode), W reference electrode and W (or Mo) working electrode. The anode gas composition during electrolysis in the NdF_3 + PrF_3 + LiF + Nd_2O_3 + Pr_6O_{11} electrolyte at 1050 °C was also analysed [6,7,17]. By applying different electrochemical techniques, we succeeded in obtaining solid Nd metal and Nd-Pr metal composition on the cathodes used from the oxide-fluoride electrolyte at 1050 °C [6,7,17].

Continuing the series on fundamental studies on selective Nd and Pr electrodeposition, with this work, we build on experiments and theory, allowing us to construct a ternary phase diagram for the liquidus temperatures of the chosen fluoride based molten salts

(NdF_3 + PrF_3 + LiF). This step was necessary to obtain an improved prediction of the optimal electrolyte constitution. To address the efficiency of the electrolyte system composition, as well as the optimal process conditions, the concentration of the REO added to the fluoride based NdF_3 + PrF_3 + LiF electrolyte was varied in order to precisely incorporate adjustable parameters, which should favour more deposited neodymium and praseodymium metal remaining on the inert working substrate. Finally, we chose low-deposition overpotential to suppress greenhouse gas emissions and to achieve high-purity Nd and Pr metal production.

2. Materials and Methods

The electrolyte was prepared by premelting the components. LiF powder was additionally dried for 24 h at 250 °C and then mixed with the other components in a vacuum induction furnace, which can be operated under overpressure. The molten melt was heated at 1050 °C. An Ar atmosphere of 1900 mbar was applied in the furnace to restrain the evaporation of fluorides. Following this homogenisation step, the electrolyte was placed in a high-purity graphite crucible with the rare earth oxides, which were dried at 120 °C for 24 h.

In order to study the effect of REO content on the electrochemical behaviour and co-deposition of Nd and Pr in molten fluoride, 45.5 wt.% NdF_3 + 45.5 wt.% PrF_3 + 9 wt.% LiF was used as the base electrolyte. REOs were added into the prepared molten salt mixture in quantities necessary to maintain the REO concentration at 1 wt.%, 2 wt.% or 4 wt.% in the molten salt electrolyte (Table 1).

Table 1. Electrolyte composition.

Component	Weight Percentage (wt.%)			Molar Ratio (mol%)			Manufacturer
NdF_3	45.5			28.16			Treibacher Industries (Carinthia, Austria) All ≥ 99.5%
PrF_3	45.5			28.63			
LiF	9.0			43.21			
Nd_2O_3	0.5	1.0	2.0	0.19	0.37	0.74	
Pr_6O_{11}	0.5	1.0	2.0	0.06	0.12	0.24	

In order to safely discharge the hazardous gases that evolved during the electrochemical experiments, the crucible for the electrolyte was placed in a steel cell, and argon was constantly circulated through the cell at a rate of 3 L/min [6,17]. This atmosphere also prevents the system from oxidising. Tungsten wires were used as working and reference electrodes, with a glassy carbon rod as a counter electrode. Electrodes were exchanged through the cell lid through a swag lock system without the gas escaping.

The details about the experimental cell setup for the electrochemical measurement procedure were previously reported [6,7]. The remaining exhaust gas was precleaned using wash bottles before it was fed into the exhaust system. Electrochemical measurements were conducted at a working temperature of 1050 °C, which was monitored via a type-B thermocouple. An IviumStat potentiostat (5 A/10 V; Ivium Technologies, Eindhoven, The Netherlands) was used for electrochemical measurements: cyclic voltammetry (CV using various scan rates in the range of 50–300 mV/s), square-wave voltammetry (SWV) and chronopotentiometry (deposition experiments were carried out in constant potentiostatic mode for up to 240 min). After the experiments, the working electrode was pulled out from the molten salt, cooled down to room temperature inside the cell under the Ar atmosphere and prepared for EPMA and X-ray diffraction (XRD) analyses. Electron probe microanalysis (EPMA) was used to observe and determine the phases formed during the deposition, as well as their compositions. A JEOL JXA-8530F electron microprobe (Tokyo, Japan) equipped with a Schottky field emission cathode was used for the EPMA analyses. Phases of the deposits on the working electrodes were identified using XRD with a Philips PW 1050 powder diffractometer (Philips, Delft, The Netherlands) at room

temperature with Ni-filtered CuKα radiation (λ = 1.54178 Å) and a scintillation detector within the 2θ range of 20–85° in steps of 0.05° and a scanning time of 5 s per step. The sample preparation method varied depending on the type of analysis. For EPMA analysis, the samples were first embedded into an acrylic resin and then polished with emery paper (600, 1000, and 2000). For XRD analysis, solidified electrolyte was mechanically removed from the cathode surface.

3. Results and Discussion

In an effort to develop a more efficient electrochemical technique to obtain Nd and Pr metals from a fluoride electrolyte system, a ternary diagram of the liquidus temperatures of the NdF_3-PrF_3-LiF system was constructed. To confirm and expand these scarce findings regarding the NdF_3-PrF_3-LiF ternary system, the system was modelled in well-known and available thermodynamical software, *FactSage*. The main challenge in creating ternary phase diagrams is the lack of thermodynamic data and databases. Because the activities of these compounds are not known, an ideal liquid solution was created as a private database through the *Solution* module. This private database was then used for construction of the phase diagram via the *Phase Diagram* module. All three compounds and their data for the liquid phase were added to the newly created solution as functions. Based on these data, a solution was created using the *One-lattice R-K/Muggianu only* model, followed by inclusion of the end members. The resulting database was used to generate the phase diagram, as shown in Figure 1.

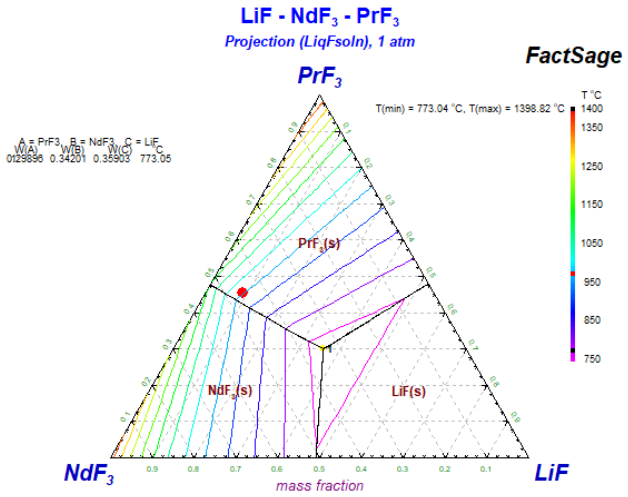

Figure 1. Phase diagram of NdF_3-PrF_3-LiF modelled by ideal solution in *FactSage*. The red circle represents the composition of the electrolyte used in this study.

The chosen composition for experimental work consisting of 45.5 wt.% NdF_3, 45.5 wt.% PrF_3 and 9 wt.% LiF is marked by a red circle in Figure 1. It clearly shows that the melting temperature of this electrolyte is approximately 970 °C, which is also in agreement with the work of Liu [27]. The phase diagram modelled here can serve as a useful first insight into system behaviour and choice of electrolyte composition. Herewith, the issues related to inappropriate composition and high mixture melting temperatures of the mixture required for process realization can be avoided.

It is generally agreed that the rare earth oxide (REO) concentration in fluoride electrolyte is important for smooth operation during electrolysis processes. However, in the electrodeposition of Nd and Pr, modelling of the oxide-fluoride based molten salt electrolyte composition is becoming increasingly important. An base electrolyte composition of 45.5 wt.% NdF_3 + 45.5 wt.% PrF_3 + 9 wt.% LiF and a melting temperature of 1050 °C were chosen, as suggested by the constructed ternary phase diagram. At the working temperature of 1050 °C, the system is in a liquid state, making it suitable for the molten salt electrolysis process.

To gather general information on the reduction processes of the Nd(III) and Pr(III) cations, cyclic voltammetry was performed with different sweep rates on W working substrate in the chosen fluoride melt composition at 1050 °C (Figure 2). Clear indications of four distinct regions of cathodic/anodic activities were observed in the potential range up to 1.000 V negative to the open circuit potential of the W working electrode (I/I′, II/II′, III/III′ and IV/IV′), with each cathodic current wave as a prerequisite for its anodic counterpart. Similar results were observed under the same conditions in our previous studies on the electrodeposition of neodymium and praseodymium from fluoride melts of similar composition [6,7]. Both cathodic and anodic peak currents increased with increasing sweep rates, but the peak potentials did not change substantially, indicating that the results obtained from this electrolyte are in agreement with those reported previously [6,7,17]. This suggests that data provided by the constructed ternary phase diagram achieve satisfactory prediction for selection of melt composition.

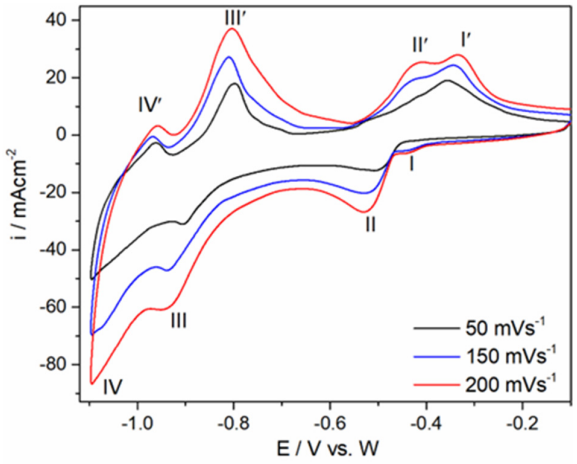

Figure 2. CVs recorded on W working electrode in NdF_3 + PrF_3 + LiF electrolyte with initial potential (E_i) = −0.100 V to cathodic end potential (E_c) = −1.100 V vs. W obtained with different sweep rates at 1050 °C.

In order to provide further insight into the Nd-Pr co-deposition process and increase its efficiency, cyclic voltammetry was performed with varying REO concentrations and scanning rates in the used electrolytes. Experiments were conducted with the W working electrode immersed in the 45.5 wt.% NdF_3 + 45.5 wt.% PrF_3 + 9 wt.% LiFbased electrolyte at 1050 °C with different REO concentrations added (Figure 3). Again, the cathodic/anodic current waves (I/I′) reflected Nd^{3+}/Nd^{2+} ion redox transitions, cathodic current wave (II) and its anodic counterpart (II′) deposition/dissolution of neodymium metal, as well as current wave (III/III′) electrochemical deposition/dissolution of Pr(III)/Pr(0). A steep increase in the current observed at potentials more negative than −0.950 V in the cathodic region should correspond to Li deposition. The current wave observed in the reverse scan counterpart should correspond to Li anodic dissolution.

Details regarding electrochemical steps of Nd and Pr cations to metals at the working cathode in the molten fluoride salts are much more complex and are discussed elsewhere [6,7,17]. Square-wave voltammetry (SWV) was employed to confirm the redox transitions of Nd and Pr cations to their metal forms during electrodeposition in fluoride based molten salt enriched with REO (Supplementary Materials Figure S1 shows the SWV results obtained on W working electrode from the fluoride melt enriched with REO). It was established that within the applied electrochemical potential range, voltammograms obtained on the same working electrodes in the molten neodymium/praseodymium fluoride based electrolytes with REO added should be qualitatively similar, whereas the currents can vary appreciably. However, some of the reduction peaks (cathodic peaks I and III), especially in the electrolytes with 0.5 wt.% Nd_2O_3 + 0.5 wt.% Pr_6O_{11} added to the base electrolyte, were not well pronounced. For example, cathodic peak (I) is not well

pronounced, probably because the next process (represented by reduction current wave II) started while the previous process (described by current wave I) was still fading away. Due to close values of the reduction potentials for reactions Nd(III) → Nd(II) and Nd(II) → Nd(0), the cathodic current wave (II) partially masks current wave (I). This is in accordance with previous literature reports [11]. It was also reported that in order to obtain ideally shaped individual current waves by cyclic voltammetry in molten salt systems, as in the case of redox transitions of Nd and Pr cations, interactions must be separated by at least 177 mV in the potential scans [11]. In our study, the reduction potentials of Nd(II) ions into Nd metal and the reduction potential of the redox process of Pr(III) ions were closer. This is consistent with the results reported in the literature on molten fluorides [5–7].

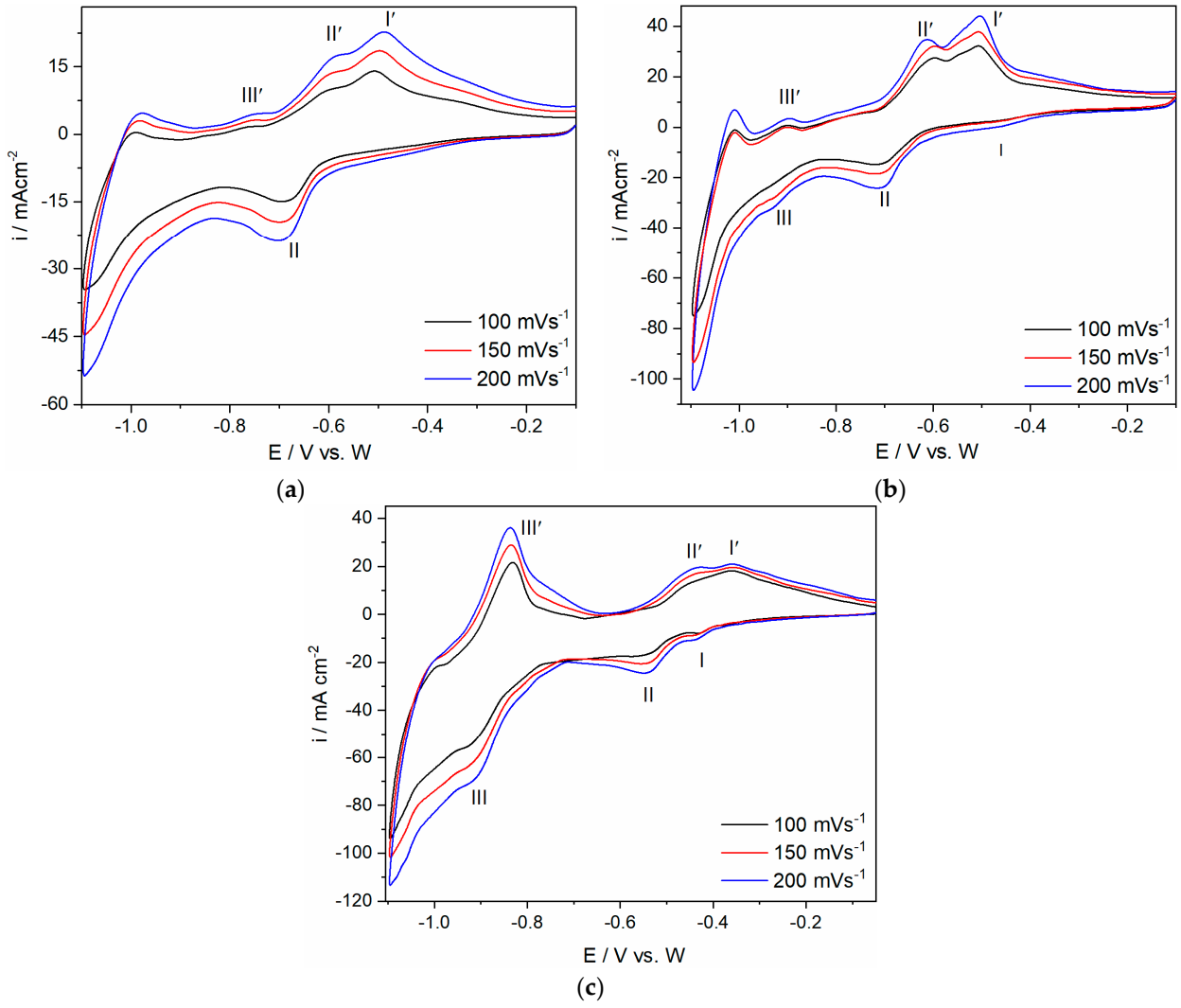

Figure 3. Cyclic voltammograms recorded on W working electrode; potential range: E_I = −0.100 V to Ec = −1.100 V vs. W. The voltammograms were obtained with different sweep rates at 1050 °C in 45.5 wt.% NdF_3 + 45.5 wt.% PrF_3 + 9 wt.% LiF electrolyte with different RE oxide concentrations added: (**a**) 0.5 wt.% Nd_2O_3 + 0.5 wt.% Pr_6O_{11}; (**b**) 1 wt.% Nd_2O_3 + 1 wt.% Pr_6O_{11}; (**c**) 2 wt.% Nd_2O_3 + 2 wt.% Pr_6O_{11}.

In the CV results recorded at various sweep rates (100–200 mVs^{-1}) in the chosen basic electrolyte with different concentrations of Nd_2O_3 and Pr_6O_{11} at 1050 °C (Figure 3), the peak potentials did not exhibit a strong dependence on the applied sweep rates, which is an indication of reversible system behaviour, as previously reported [6,7].

These cyclic voltammograms are consistent with those recorded under the same conditions in the molten fluoride electrolyte composed of 63.17 wt.% NdF_3 + 20.96 wt.% PrF_3 + 12.02 wt.% LiF + 1 wt.% Pr_6O_{11} + 1 wt.% Nd_2O_3 [6,7]. Comparison of the presented voltammograms suggests that the observed redox couples associated with the above cited electrochemical reactions are in agreement with those recorded in our previous studies [6,7]. With respect to electrolyte composition, it should be noted that the experimentally recorded current densities of the redox processes obtained by CV under the same conditions in the previously reported electrolyte with higher LiF concentration (NdF_3 + PrF_3 + 12.02 wt.% LiF) were substantially lower than those in the electrolyte with a lower concentration of LiF (NdF_3 + PrF_3 + 9 wt.% LiF). This can be attributed to the LiF content in the electrolyte used to dissolve REO because the content of different salts in molten fluoride determines the solubility of REO [8,21,22,28–30]. In the basic electrolyte, mass exchange takes place among the added oxides and existing rare earth fluorides; as a result, an equilibrium chemical composition is formed in the molten electrolyte [8]. Therein, LiF acts as a dilution agent for the melts, but an increase in LiF concentration above a certain value was observed to reduce the REO solubility [28,31,32]. It seems that LiF acts as a donor of F^-, which should improve the electrolyte conductivity and help reduce the electrolyte's viscosity while simultaneously reducing the solubility of rare earth oxides in the electrolyte [28]. It was suggested that the solubility of rare earth oxides in the electrolyte is limited (approximately 3–5%) and that the optimal LiF concentration in fluoride based baths is up to 12.5 wt.% [28]. Upon entering the molten salt, Nd_2O_3 dissolves in the presence of NdF_3 and excess F^-; as a result, neodymium oxyfluoride is formed [6,21]. Neodymium oxyfluoride then reacts to form NdO^+ and Nd^{3+}, which are converted to metallic Nd at the cathode [6,21,23]. In addition, Nd(III) ions with a surplus of F^{-} ions form a neodymium fluoride complex. The neodymium fluoride complexes also participate at the cathode as a source of Nd metal during electrolysis. Which of the corresponding species are predominantly involved as a source of neodymium metal on the working electrode substrate is determined by the applied electrode potential, current density and molar ratio of neodymium oxyfluoride ions/neodymium fluoride complexes [6,7]. Relatively similar solubility of praseodymium oxide in fluoride based electrolyte is closely related to the similarities in the atomic structure of Pr and Nd [8]. When praseodymium oxide is dissolved in neodymium fluoride or corresponding praseodymium fluoride electrolyte, solubility is not significantly affected [8]. The addition of REO to the fluoride based melt at a certain melt temperature after dissolution induces the formation of various Re-O-F or/and Re-F complex groups [22,33]. This means that the increase in cathodic/anodic current peaks related to Nd and Pr redox transitions is due to the presence of a number of neodymium/praseodymium complexes in the melt, leading to rare earth metals deposited on the cathode.

In order to obtain higher quantities of neodymium and praseodymium metals from Nd and Pr oxyfluoride melts, potentiostatic deposition was performed at −0.950 V and −0.900 V vs. W. In the initial investigation performed with 45.5 wt.% NdF_3 + 45.5 wt.% PrF_3 + 9 wt.% LiF + 0.5 wt.% Nd_2O_3 + 0.5 wt.% Pr_6O_{11} electrolyte on W cathode, we showed that CV and SWV behaviour can reliably predict the Nd and Pr redox transitions, as well as Nd-Pr co-deposition [34]. CV experiments (Figures 2 and 3) have proven that such a cathodic end potential is negative enough to sustain praseodymium and neodymium electrodeposition but not negative enough to induce lithium deposition. The chronoamperometric i = f (t) responses to the constant potential applied to the W working electrode for the same time at 1050 °C in the fluoride based electrolyte 45.5 wt.% NdF_3 + 45.5 wt.% PrF_3 + 9 wt.% LiF with different REO contents varied (Figure 4). For example, deposition from the electrolyte with total of 2 wt.% RE oxides maintained a descending deposition current density, with an average value of ≈ -12 mAcm^{-2} (Figure 4a). In the electrolyte with a total of 4 wt.% RE oxides added, the deposition current density increased to an average value of ≈ -16 mAcm^{-2} (Figure 4b). After two hours of deposition, with all other conditions held constant, the value of the deposition current used in the electrolyte with 4 wt.% REO added was ≈ 33% greater than that in the electrolyte with a lower REO concentration.

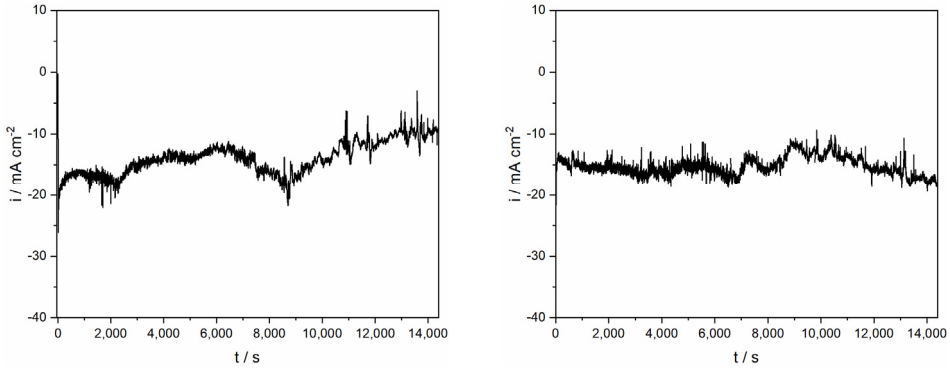

Figure 4. Potentiostatic deposition on W working electrode from the 45.5 wt.% NdF_3 + 45.5 wt.% PrF_3 + 9 wt.% LiF electrolyte at 1050 °C for 4 h; (**a**) with 1 wt.% Nd_2O_3 + 1 wt.% Pr_6O_{11} added at a constant potential of −0.950 V vs. W; and (**b**) with 2 wt.% Nd_2O_3 + 2 wt.% Pr_6O_{11} added at a constant potential of −0.900 V vs. W.

EPMA mapping of the samples after deposition from the fluoride based electrolyte enriched with REO is shown in Figures 5 and 6. Neodymium and praseodymium metal deposits on W cathode were confirmed (Figures 5 and 6). Most of the neodymium and praseodymium metal is distributed in the area close to the working electrode substrate (Figure 5a,b and Figure 6a,b). This area represents a thin layer of Nd and Pr metallic phase deposited on the electrode surface. Oxygen and fluoride are present in the lowest recorded concentrations in these areas (Figures 5d and 6d), which suggests that large fractions of the oxyfluorides complexes formed by either oxide or fluoride exchange with available fluorides or oxides in the electrolyte were converted into metallic neodymium or/and praseodymium. EPMA quantification results (Figures 5c and 6c) showing the area from the cathode surface up to the bulk solution indicate a high concentration of Nd and Pr metals (approximately 40 mass% neodymium and 40 mass% Pr), suggesting that the metals were deposited at the cathode.

The area with the highest concentration of fluoride corresponds to the melt residue phase, as it was shown in Figures 5e and 6e. The EPMA analysis data show that the oxygen is mainly situated in the electrolyte (Figures 5d and 6d).

It is apparent that the distance between the cathode surface and the beginning of the melt residue shown in Figure 5a,b and Figure 6a,b is different (in Figure 5, it is ≈ 60 µm, and in Figure 6, it is ≈ 80 µm). This suggests that neodymium and praseodymium metal yields increased slightly as the percentage of Pr_6O_{11} and Nd_2O_3 added was increased in the base electrolyte from 2 to 4 wt.% REO.

In order to apply XRD analysis to the working electrode after prolonged deposition, the solidified electrolyte was mechanically removed from the working electrode surface. The samples were then analysed by XRD (Figure 7a,b). Figure 7a shows an XR diffractogram of the sample obtained on a W cathode in potentiostatic mode at −0.950 V vs. W in molten NdF_3 + PrF_3 + LiF + 1 wt.% Nd_2O_3 + 1 wt.% Pr_6O_{11} electrolyte at 1050 °C after 240 min. Corresponding neodymium metal peaks were observed at 28.16°, 29.18°, 30.28°, 32.06°, 36.40°, 60.52°, 62.37°, 70.38° and 77.33° (JCPDS No. 03-065-3424). Because of the similar lattice parameters, the same peaks, with slight variation in 2θ values, were observed for praseodymium metal (JCPDS No. 01-089-2921). In addition to the strong peaks of neodymium and praseodymium metals, the characteristic peaks of NdF_2 were observed (JCPDS No. 00-033-0934). It is important to note that NdF_2 is a product of the following disproportionation reaction: Nd(0) + 2Nd(III) → 3 Nd(II). Formation of NdF_2 is unavoidable during Nd electrodeposition from fluoride based melts or halide electrolytes, as observed by other authors [6,7,11,35]. Figure 7b shows the XRD analysis of the W cathode after potentiostatic deposition in the same base electrolyte melt with 4 wt.% REO added at 1050 °C. As shown in the XR diffractogram, the cathode deposit exhibits peaks of

Nd and Pr metals, indicating a small amount of melt residue. The 2θ values for neodymium and praseodymium metal are in agreement with the previous diffractogram (Figure 7a). There are three additional, relatively strong peaks that are related to neodymium and praseodymium metals, which were observed at 48.06°, 52.37° and 71.75°. Apart from the prominent peaks corresponding to neodymium and praseodymium metals, there is a peak at 46.1°, referred to as Nd metal (JCPDS No. 03-065-3424). The peaks related to LiF (JCPDS No. 01-072-1538) were hardly detectable on the electrode surface. The samples obtained after potentiostatic deposition clearly verified that rare earth metals were produced on the W working electrode.

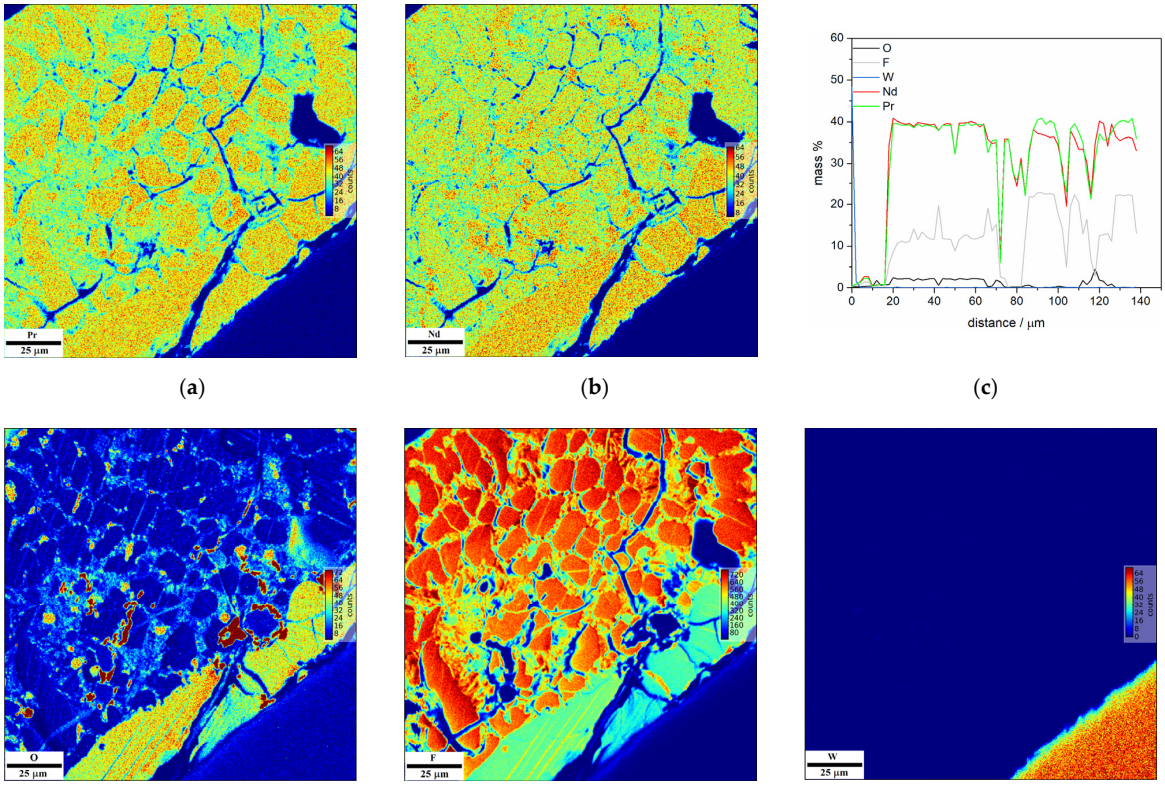

(**a**) (**b**) (**c**)

(**d**) (**e**) (**f**)

Figure 5. EPMA mapping of the sample after deposition at −0.950 V vs. W on a W cathode from molten NdF_3 + PrF_3 + LiF + 1 wt.% Nd_2O_3 + 1 wt. %Pr_6O_{11} electrolyte for 240 min. at 1050 °C, showing distribution: (**a**) Pr; (**b**) Nd; (**c**) concentration profile (mass%); (**d**) O; (**e**) F; (**f**) W.

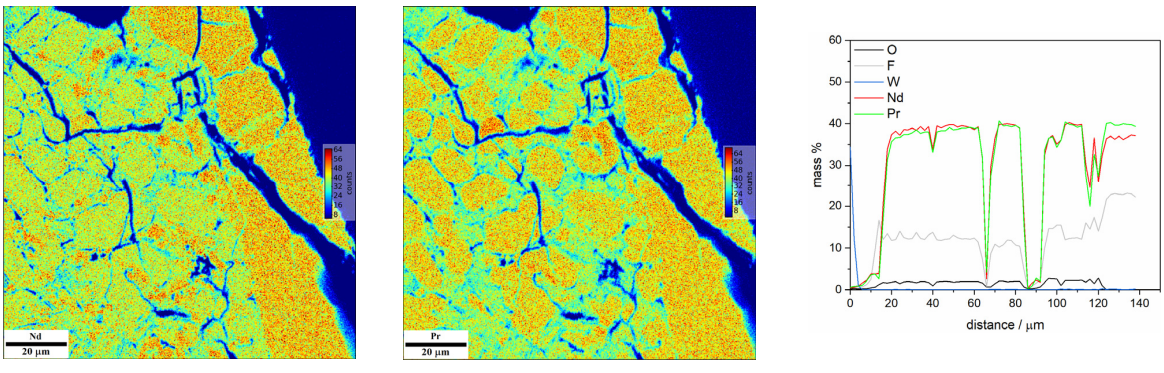

(**a**) (**b**) (**c**)

Figure 6. *Cont.*

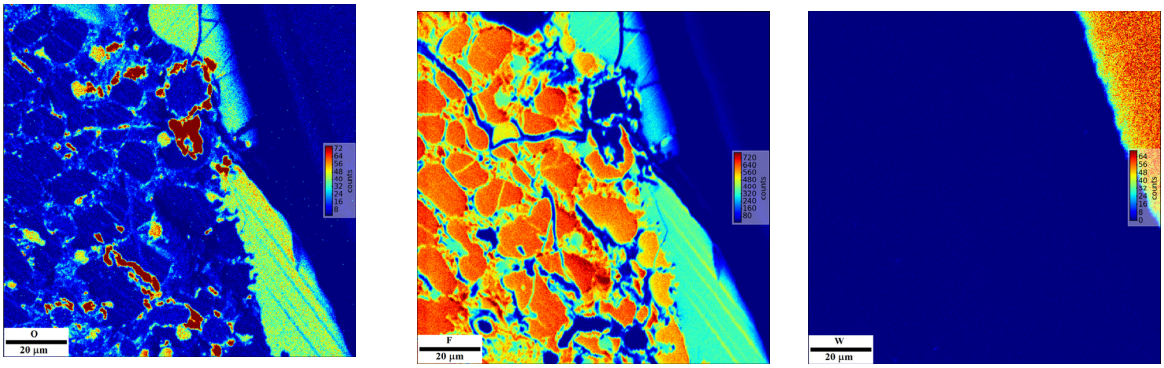

(**d**) (**e**) (**f**)

Figure 6. EPMA mapping of the sample after deposition at −0.900 V vs. W on a W cathode from molten NdF_3 + PrF_3 + LiF + 2 wt.% Nd_2O_3 + 2 wt.% Pr_6O_{11} electrolyte for 240 min. at 1050 °C; showing distribution: (**a**) Pr; (**b**) Nd; (**c**) concentration profile (mass%); (**d**) O; (**e**) F; (**f**) W.

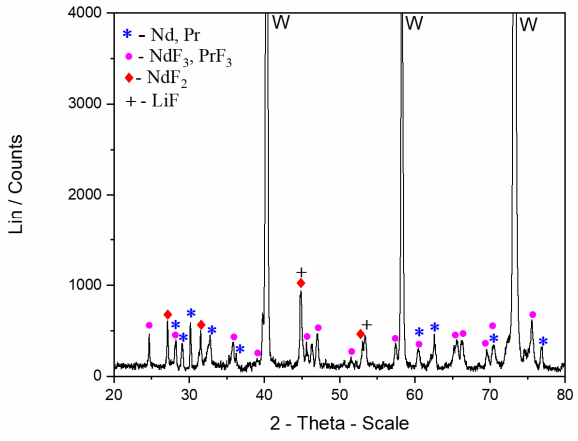

(**a**)

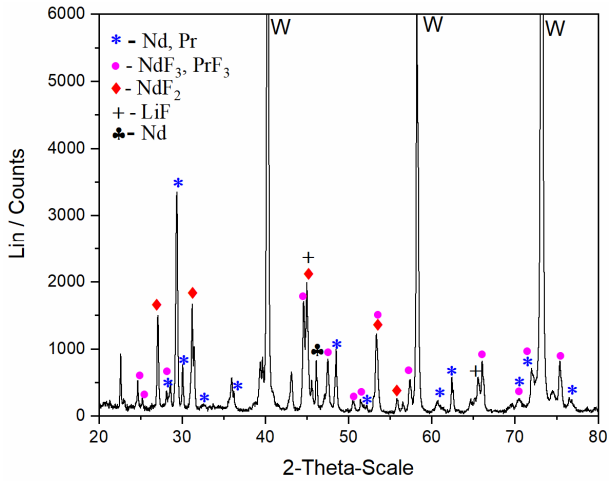

(**b**)

Figure 7. (**a**) X-ray diffraction analysis of the deposit obtained after deposition at −0.950 V vs. W on a W cathode from molten NdF_3 + PrF_3 + LiF + 1 wt.% Nd_2O_3 + 1 wt.% Pr_6O_{11} electrolyte for 240 min. at 1050 °C (the solidified electrolyte was removed from the electrode). (**b**) X-ray diffraction analysis of the deposit obtained after deposition at −0.900 V vs. W on a W working electrode from molten NdF_3 + PrF_3 + LiF + 2 wt.%Nd_2O_3 + 2 wt.%Pr_6O_{11} electrolyte for 240 min at 1050 °C (the solidified electrolyte was removed from the electrode).

The results from this study, as well as those of our previous work, validate our choice of the electrolyte composition, as well as the applied deposition potentials. Peaks corresponding to NdF_2 observed in the diffractograms imply that the amount of NdF_2 increases with increased addition of rare earth oxides. Although the reaction of disproportionation decreases the yield of neodymium metal remaining on the working electrode surface, the efficiency of the electrolysis process was improved with REO addition. This is in accordance with the EPMA results (Figures 5 and 6), which demonstrated that the quantities of Nd and Pr metals on the cathode are increased with increased REO addition. It is evident that the results of the XRD analyses are comparable those reported in our previous studies, confirming the applicability of the calculated phase diagram to the electrolyte composition used in the present work [6,7,17].

4. Conclusions

A ternary phase diagram was calculated for an electrolyte composed of lithium, neodymium and praseodymium fluorides. Based on the diagram, an electrolyte melting temperature of 1050 °C was chosen and was shown to be optimal for this deposition application. Thus, the proposed ternary diagram showed potential for future applications of this system.

Electrochemical co-deposition of neodymium and praseodymium was performed in basic 45.5 wt.% NdF_3 + 45.5 wt.% PrF_3 + 9 wt.% LiF molten salts enriched with 1, 2 or 4 wt.% Pr_6O_{11} + Nd_2O_3 at 1050 °C. We confirmed that for all chosen concentrations of REO, electrodeposition of Nd proceeds as a two-step reduction process, whereas Pr deposition plays out in a one-step reduction process.

Experimentally measured current densities of the deposition processes performed at constant working electrode potentials (−0.950 V, and −0.900 V vs. W) in the fluoride based electrolyte with lower REO content were substantially lower than those obtained under the same conditions in the electrolyte with higher content of REO.

XRD and EPMA analyses of the samples of solidified deposits and surrounding electrolyte confirmed that electrolysis in the melts with higher REO content (for example, 4 wt.% REO) resulted in a more effective deposition process, as reflected by higher Nd and Pr metal yields on the working electrode under similar conditions.

The ever-increasing demand for high-performance magnets will make the recycling of NdFeB magnets inevitable in the future. Our investigations represent an important step with respect to further development of such recycling processes.

Supplementary Materials: The following are available online at: https://www.mdpi.com/article/10.3390/met12071204/s1, Figure S1: (a) SWVs obtained with different frequencies on W working electrode: pulse height: 25 mV; potential step: 1 mV; Variation of the peak current density vs. the square root of the frequency for: (b) Peak II; (c) Peak III. Electron transfer numbers were calculated based on the half-peak width recorded by SWV (embedded in the picture).

Author Contributions: V.S.C.: methodology, writing—original draft preparation; D.F.: experimental execution; N.M.V.: investigation, writing—original draft preparation; K.M.-N.: construction of the phase diagram; T.S.B.: XRD data curation; B.F. and J.N.J.: supervision, writing—review and editing; B.F. (RWTH Aachen University): funding acquisition. All authors discussed the results and commented on the manuscript. All authors have read and agreed to the published version of the manuscript.

Funding: Part of this research was supported by funds of the bilateral research project (ID:451-03-01344/2020-09/8) supported by the Ministry of Education, Science and Technological Development of the Republic of Serbia and German Academic Exchange Service (DAAD).

Institutional Review Board Statement: Not applicable.

Informed Consent Statement: Not applicable.

Data Availability Statement: Not applicable.

Acknowledgments: Vesna S. Cvetković and Nataša M. Vukićević acknowledge the financial support for the investigation received from the Ministry of Education, Science and Technological Development of the Republic of Serbia (Grant No. 451-03-68/2022-14/200026).

Conflicts of Interest: The authors declare no conflict of interest.

References

1. Balaram, V. Rare earth elements: A review of applications, occurrence, exploration, analysis, recycling, and environmental impact. *Geosci. Front.* **2019**, *10*, 1285–1303. [CrossRef]
2. Yasuda, K.; Kondo, K.; Nohira, T.; Hagiwara, R. Electrochemical Formation of Pr–Ni Alloys in LiF–CaF_2 –PrF_3 and NaCl–KCl–$PrCl_3$ Melts. *J. Electrochem. Soc.* **2014**, *161*, D3097–D3104. [CrossRef]
3. Yang, Y.; Walton, A.; Sheridan, R.; Güth, K.; Gauß, R.; Gutfleisch, O.; Buchert, M.; Steenari, B.-M.; Van Gerven, T.; Jones, P.T.; et al. REE Recovery from End-of-Life NdFeB Permanent Magnet Scrap: A Critical Review. *J. Sustain. Metall.* **2017**, *3*, 122–149. [CrossRef]
4. Yin, X.; Martineau, C.; Demers, I.; Basiliko, N.; Fenton, N.J. The potential environmental risks associated with the development of rare earth element production in Canada. *Environ. Rev.* **2021**, *29*, 354–377. [CrossRef]
5. Yang, Y.; Lan, C.; Guo, L.; An, Z.; Zhao, Z.; Li, B. Recovery of rare-earth element from rare-earth permanent magnet waste by electro-refining in molten fluorides. *Sep. Purif. Technol.* **2020**, *233*, 116030. [CrossRef]
6. Cvetković, V.S.; Feldhaus, D.; Vukićević, N.M.; Barudžija, T.S.; Friedrich, B.; Jovićević, J.N. Investigation on the electrochemical behaviour and deposition mechanism of neodymium in NdF_3–LiF–Nd_2O_3 melt on Mo electrode. *Metals* **2020**, *10*, 576. [CrossRef]
7. Cvetković, V.S.; Feldhaus, D.; Vukićević, N.M.; Barudžija, T.S.; Friedrich, B.; Jovićević, J.N. Electrochemical Study of Nd and Pr Co-Deposition onto Mo and W from Molten Oxyfluorides. *Metals* **2021**, *11*, 1494. [CrossRef]
8. Senanu, S.; Ratvik, A.; Gudbrandsen, H.; Martinez, A.; Støre, A.; Gebarowski, W. Dissolution and Online Monitoring of Nd and Pr Oxides in NdF_3–PrF_3–LiF Electrolytes. *Metals* **2021**, *11*, 326. [CrossRef]
9. Martinez, A.M.; Kjos, O.; Skybakmoen, E.; Solheim, A.; Haarberg, G.M. Extraction of Rare Earth Metals from Nd-based Scrap by Electrolysis from Molten Salts. *ECS Trans.* **2012**, *50*, 453–461. [CrossRef]
10. Joo, M.H.; Park, S.J.; Hong, S.M.; Rhee, C.K.; Sohn, Y. Electrochemical Recovery and Behaviors of Rare Earth (La, Ce, Pr, Nd, Sm, Eu, Gd, Tb, Dy, Ho, Er, Tm, and Yb) Ions on Ni Sheets. *Materials* **2020**, *13*, 5314. [CrossRef]
11. Shen, D.; Akolkar, R. Electrodeposition of Neodymium from $NdCl_3$-Containing Eutectic LiCl–KCl Melts Investigated Using Voltammetry and Diffusion-Reaction Modeling. *J. Electrochem. Soc.* **2017**, *164*, H5292–H5298. [CrossRef]
12. Tang, H.; Pesic, B. Electrochemistry and the mechanisms of nucleation and growth of neodymium during electroreduction from LiCl-KCl eutectic salts on Mo substrate. *J. Nucl. Mater.* **2015**, *458*, 37–44. [CrossRef]
13. Castrillejo, Y.; Bermejo, M.R.; Arocas, P.D.; Martínez, A.M.; Barrado, E. The electrochemical behaviour of the Pr(III)/Pr redox system at Bi and Cd liquid electrodes in molten eutectic LiCl–KCl. *J. Electroanal. Chem.* **2005**, *579*, 343–358. [CrossRef]
14. Nohira, T.; Kambara, H.; Amezawa, K.; Ito, Y. Electrochemical Formation and Phase Control of Pr-Ni Alloys in a Molten LiCl-KCl-$PrCl_3$ System. *J. Electrochem. Soc.* **2005**, *152*, C183–C189. [CrossRef]
15. Liu, X.; Huang, C.; Li, B. The effects of NdF_2 on current efficiency of Nd extraction from NdF_3-LiF-Nd_2O_3 melts. *Mater. Trans.* **2017**, *58*, 395–399. [CrossRef]
16. Massot, L.; Gibilaro, M.; Nicaise, J.; Chamelot, P. Electrochemical behaviour of Lanthanum fluoride and Praseodymium fluoride on inert and reactive electrodes in molten LiF-CaF_2. *J. Fluor. Chem.* **2021**, *246*, 109797. [CrossRef]
17. Cvetković, V.S.; Vukićević, N.M.; Feldhaus, D.; Barudžija, T.S.; Stevanović, J.; Friedrich, B.; Jovićević, J.N. Study of Nd Deposition onto W and Mo Cathodes from Molten Oxide-Fluoride Electrolyte. *Int. J. Electrochem. Sci.* **2020**, 7039–7052. [CrossRef]
18. Yasuda, K.; Kondo, K.; Kobayashi, S.; Nohira, T.; Hagiwara, R. Selective Formation of Rare-Earth–Nickel Alloys via Electrochemical Reactions in NaCl–KCl Molten Salt. *J. Electrochem. Soc.* **2016**, *163*, D140–D145. [CrossRef]
19. Castrillejo, Y.; Bermejo, M.R.; Díaz Arocas, P.; Martínez, A.M.; Barrado, E. Electrochemical behaviour of praseodymium (III) in molten chlorides. *J. Electroanal. Chem.* **2005**, *575*, 61–74. [CrossRef]
20. Abbasalizadeh, A.; Seetharaman, S.; Venkatesan, P.; Sietsma, J.; Yang, Y. Use of iron reactive anode in electrowinning of neodymium from neodymium oxide. *Electrochim. Acta* **2019**, *310*, 146–152. [CrossRef]
21. Kwon, S.; Ryu, H.-Y.; Cho, S.-H.; Lee, J.-H. Effect of the electrolyte composition on the electrochemical behavior of Nd fluoride complex in a LiF-NdF_3-Nd_2O_3 molten salt. *J. Electroanal. Chem.* **2020**, *879*, 114751. [CrossRef]
22. Zhang, Y.N.; Li, J.; Chai, D.P.; Gao, Y.Y.; Wang, C.Z.; Hou, G.H.; Yu, Q.; Liu, L.Y.; Zhang, F.P.; Liu, X. Study on the Conductivity of Molten Salt in PrF_3-NdF_3-LiF-Pr_6O_{11}-Nd_2O_3. *Chin. Rare Earths* **2020**, *41*, 92–96.
23. Sarfo, P.; Das, A.; Young, C. Extraction and optimization of neodymium from molten fluoride electrolysis. *Sep. Purif. Technol.* **2021**, *256*, 117770. [CrossRef]
24. Milicevic, K.; Feldhaus, D.; Friedrich, B. Conditions and Mechanisms of Gas Emissions from Didymium Electrolysis and Its Process Control. In *Light Metals 2018. TMS 2018. The Minerals, Metals & Materials Series*; Martin, O., Ed.; Springer: Cham, Switzerland, 2018; pp. 1435–1441, ISBN 978-3-319-72283-2.
25. Thoma, R.E. Phase Diagrams of Binary and Ternary Fluoride Systems. In *Advances in Molten Salt Chemistry*; Springer: Boston, MA, USA, 1975; pp. 275–455.

26. Berkani, M.; Gaune-Escard, M. Study of binary systems NdF_3-MF (M = Li, Na, K): Experimental, modeling and thermodynamic computation. *MATEC Web Conf.* **2013**, *3*, 01033. [CrossRef]
27. Fangyu, L. *Fundamental Electrochemical Study on Neodymium Molten Salt Electrolysis in Fluoride Bath: Fundamental Electrochemical Study on Neodymium Molten Salt Electrolysis in Fluoride Bath*; Colorado School of Mines: Golden, CO, USA, 2019. Available online: https://hdl.handle.net/11124/173998 (accessed on 1 February 2022).
28. Zuo, Z.; Liu, Y.; Yang, X.; Liu, F. PrF_3-NdF_3-DyF_3-LiF electrolyte system for preparation of Pr-Nd-Dy alloy by electrolysis. *J. Rare Earths* **2021**, *40*, 996–1001. [CrossRef]
29. Guo, X.; Sun, Z.; Sietsma, J.; Yang, Y. Semiempirical Model for the Solubility of Rare Earth Oxides in Molten Fluorides. *Ind. Eng. Chem. Res.* **2016**, *55*, 4773–4781. [CrossRef]
30. Hu, X.; Wang, Z.; Gao, B.; Shi, Z.; Liu, F.; Cao, X. Density and ionic structure of NdF_3-LiF melts. *J. Rare Earths* **2010**, *28*, 587–590. [CrossRef]
31. Guo, X.; Sun, Z.; Sietsma, J.; Blanpain, B.; Guo, M.; Yang, Y. Quantitative Study on Dissolution Behavior of Nd_2O_3 in Fluoride Melts. *Ind. Eng. Chem. Res.* **2018**, *57*, 1380–1388. [CrossRef]
32. Ciumag, M.; Gibilaro, M.; Massot, L.; Laucournet, R.; Chamelot, P. Neodymium electrowinning into copper-neodymium alloys by mixed oxide reduction in molten fluoride media. *J. Fluor. Chem.* **2016**, *184*, 1–7. [CrossRef]
33. Lee, G.-G.; Jo, S.-K.; Lee, C.-K.; Ryu, H.Y.; Lee, J.H. Study on Electrolysis for Neodymium Metal Production. In *Rare Metal Technology 2015*; Neelameggham, N.R., Alam, S., Oosterhof, H., Jha, A., Dreisinger, D., Wang, S., Eds.; Springer International Publishing: Cham, Switzerland, 2015; pp. 249–252, ISBN 9781119078302.
34. Cvetković, V.S.; Feldhaus, D.; Vukićević, N.; Nikolić, N.D.; Friedrich, B.; Jovićević, J. Electrodeposition of Nd and Pr onto W from fluoride based melts. In Proceedings of the Meeting Point of the Science and Practice in the Fields of Corrosion, Materials and Environmental Protection, XXII YuCorr International Conference, Tara Mountain, Serbia, 13–16 September 2021; Pavlović, M., Pavlović, M., Pantović Pavlović, M., Eds.; Serbian Society of Corrosion and Materials Protection UISKOZAM: Belgrade, Serbia, 2021; pp. 157–160.
35. Huang, C.; Liu, X.; Gao, Y.; Liu, S.; Li, B. Cathodic processes of neodymium(III) in LiF-NdF_3-Nd_2O_3 melts. *Faraday Discuss.* **2016**, *190*, 339–349. [CrossRef]